Preparation and Adsorption Properties of Chitosan–Poly(acrylic acid) Nanoparticles for the Removal of Nickel Ions

Jian-Wen Wang,[1] Yi-Ming Kuo[1,2]

[1]Department of Environmental and Safety Engineering, Chung Hwa University of Medical Technology, 89 Wen-Hua 1st Street, Jen-Te Hsiang, Tainan Hsien, Taiwan
[2]Sustainable Environment Research Center, National Cheng Kung University, Tainan 70101, Taiwan

ABSTRACT: Chitosan (CS) nanoparticles with different mean sizes ranging from 100 to 195 nm were prepared by ionic gelation of CS and poly(acrylic acid) (PAA). Variations in the final solution pH value and CS : PAA volume ratio were examined systematically for their effects on nanoparticle size, intensity of surface charge, and tendency toward particle aggregation. The sorption capacity and sorption isotherms of the CS–PAA nanoparticles for nickel ions were evaluated. The parameters for the adsorption of nickel ions by the CS–PAA nanoparticles were also investigated. The CS–PAA nanoparticles could sorb nickel ions effectively. The sorption rate for nickel ions was affected significantly by the initial concentration of the solution, sorbent amount, particle size, and pH value of the solution. The samples of nanoparticles were well correlated with Langmuir's isotherm model, and the adsorption kinetics of nickel correlated well with the pseudo-second-order model. The maximum capacity for nickel sorption deduced from the use of the Langmuir isotherm equation was 435 mg/g, which was significantly higher than that of the micrometer-sized CS. © 2007 Wiley Periodicals, Inc. J Appl Polym Sci 107: 2333–2342, 2008

Key words: adsorption; chitosan; nanotechnology; self-assembly

INTRODUCTION

Metal removal or recovery from aqueous waste streams is becoming an increasingly important issue because of growing economic and environmental concerns. One of the metals released to the environment from a number of sources is nickel. Nickel is one of the most commonly occurring metals in electroplating processes, nickel batteries, alloys, steels, and also discharged effluent. It is easily absorbed if ingested and is toxic in two significant ways: it poses hazards to the neural system and also possibly causes gene mutations. Therefore, the removal of nickel from aqueous waste streams is a matter of top priority. Incidentally, nickel is also expensive, so its recovery should pay, in part or in full, for the cost of the abatement technology.

Current methods for wastewater treatment include precipitation, coagulation/flotation, sedimentation, flotation, filtration, membrane processes, electrochemical techniques, ion exchange, biological process, chemical reactions, and adsorption.[1] Each method has its merits and limitations in application. Adsorption is considered an effective and economical method for the removal of pollutants from wastewater. The adsorption process with activated carbon is attractive to many scientists because of the effectiveness of the removal of heavy-metal ions at trace quantities.[2] However, the process has not been used extensively because of its high cost. Therefore, the uses of low-cost materials as sorbents for metal removal from wastewater has been a focus. Biopolymers have been studied as adsorbents for the removal of various heavy-metal ions from water and industrial effluents because they possess a number of different functional groups, such as hydroxyls and amines, which increase the efficiency of metal-ion uptake and the maximum chemical loading possibility. Chitosan (CS), a linear polysaccharide based on a glucosamine unit, is obtained from the deacetylation of chitin, which is the major component of crustaceans shells. CS has received considerable interest for heavy-metal removal because of its excellent metal-binding capacities and its low cost compared to activated carbon.[3] Most commercialized or developed CS is submicrometer to micrometer sized and has large internal porosities to ensure adequate surface area for adsorption. However, diffusion limitations within the particles lead to a decrease in the

adsorption rate and available capacity. To reduce this resistance to mass transfer, CS-based nanoparticles have been developed to reduce its crystallinity and size to favor the sorption rate.[4] CS nanoparticles should have the following advantages:[5] (1) CS nanoparticles can be produced in large quantity with the sol–gel method; (2) it can be expected that the adsorption capacity for CS nanoparticles will be higher because of their larger surface area and highly active surface sites; and (3) it is possible that the uptake process occurs via external adsorption, which results in a very short adsorption time. Qi and Xu[6] studied the sorption behavior of CS–tripolyphosphate nanoparticles for lead and found that the adsorption capacities for lead (398 mg/g) were very high due to the large surface area. Chang and Chen[7] studied the sorption behavior of carboxymethylated CS-bound Fe_3O_4 nanoparticles for Acid Orange 12 and found that the adsorption capacities for Acid Orange 12 (1883 mg/g) were also extremely high. They also found that CS-bound Fe_3O_4 nanoparticles were shown to be efficient for the removal of Cu(II) ions at pH > 2.[8] In particular, the adsorption rate was so fast that equilibrium was achieved within 1 min due to the absence of internal diffusion resistance.

Self-assembly is a process whereby atoms, molecules, and molecular aggregates organize and arrange themselves through weak and noncovalent forces such as hydrogen bonding, electrostatic interactions, and hydrophobic forces into stable and structurally well-defined functional entities at the mesoscale and nanoscale dimensions. Self-assembly combining two oppositely charged polyelectrolytes into nanoparticles can be achieved by ionic gelation. For example, negatively charged DNA can form nanoparticles with positively charged polymers, such as CS[9] and polyethylenimine.[10] So far, there have been many reports on the formation of CS nanoparticles through the ionic gelation process. Bodmeier et al.[11] first reported the ionotropic gelation of CS with tripolyphosphate for drug encapsulation. Lin et al.[12] prepared nanoparticles composed of CS/poly(γ-glutamic acid) and evaluated their permeability through Caco-2 cells. Douglas and Tabrizian[13] introduced a new procedure for the preparation of alginate–CS nanoparticles and examined several experimental parameters in relation to their formation and characteristics. Alonso-Sande et al.[14] reported the formation of a new type of nanoparticle made of hydrophilic polysaccharides, CS, and glucomannan and studied their potential for the association and delivery of proteins. Kabanov et al.[15] indicated that these biomedical nanoparticles consisted of a long-host molecule sequentially complexed with shorter guest polyions of opposite charge, according to a zip mechanism. In addition, Schatz et al.[16] demonstrated that the influence of the molecular weight of compo-

nents on their particles sizes could be well explained by the chain-length ratios of the two polymers. Therefore, high-molecular-weight CS was used as a host material complexed with short guest polyions of poly(acrylic acid) (PAA) in this study. To avoid irreversible flocculation occurring with a dropwise approach for the polyelectrolyte complex particle, a one-shot addition of polyelectrolyte was used in this study when the mixing ratios were close to unity. This one-shot process was easy to perform, was insensitive to the mixing order of reactants, and led to highly stable, charged, biopolymer-based colloids.

The aim of this study was to synthesize CS nanoparticles by the ionic gelation of high-molecular CS and PAA. The sorption capacity and sorption isotherms of CS–PAA nanoparticles for nickel ions were also evaluated. The influences of various experimental conditions, such as the initial concentration of the solution, sorbent amount, particle size, and pH value of the solution, on the adsorption capacity of the nanoparticles for nickel ions were investigated. The equilibrium sorption capacities for the nickel on the nanoparticles were studied with the adsorption isotherm technique. The experimental data were then fitted into the Langmuir and Freundlich equations. This information will be useful for further applications of system design in the treatment of practical waste effluents.

EXPERIMENTAL

Materials

CS (weight-average molecular weight ≈ 40,0000) was purchased from Fluka (Buchs, Switzerland). The degree of deacetylation was about 88%, as determined by an IR method. PAA (viscosity = 8000–12000 cp) was obtained from Showa (Tokyo, Japan). Acetic acid was obtained from Fluka. Nickel nitrate was purchased from Riedel-de Haën (Seelze, Germany). All other reagents were analytical grade and were used without further purification.

Preparation of the CS–PAA nanoparticles

CS–PAA nanoparticles were prepared in our previous study.[17] To simplify the preparation procedure, the incubation processes were modified. Briefly, CS flakes were measured and dissolved in an acetic acid solution at a concentration of 0.01 wt % with 1% acetic acid; the pH was then raised to 4.5 with 10N sodium hydroxide. The PAA solution was also dissolved in deionized water at 1%, and the pH of the prepared PAA solution was 4.7. CS–PAA nanoparticles formed spontaneously on the dropwise addition of an aqueous PAA solution into CS solution at a dropping rate of 1 drop/s with a syringe connected

to a peristaltic pump. The final pH value of the CS–PAA complex was adjusted to 3 by 1M hydrochloride acid and then to 5 and 7 by 1M sodium hydroxide. Different mean sizes of nanoparticles were obtained by adjustment of the ratio of PAA to CS. Nanoparticles were purified by centrifugation at 9000 × g for 30 min. The supernatants were discarded, and the CS–PAA nanoparticles were rinsed extensively with distilled water to remove any sodium hydroxide residues; the nanoparticles were kept at −55°C for 1 day and then freeze-dried again before further use or analysis.

Fourier transform infrared/attenuated total reflectance (FTIR–ATR) spectrum analysis

FTIR spectra were measured with a Thermo Nicolet (Madison, WI) Nexus 470 FTIR–ATR spectrometer to determine the chemical interaction between CS and PAA.

Transmission electron microscopy (TEM) observation

A Hitachi HF-2000 field emission transmission electron microscope (Tokyo, Japan) was used to observe the morphology of the nanoparticles. The samples were placed on a copper grid coated with a carbon membrane at room temperature without staining.

Size distribution and ζ potential analysis

Mean diameter size distribution and ζ potential of the CS–PAA nanoparticles were determined with a Malvern Zetasizer 3000 HS (Herrenberg, Germany). Each sample of the nanoparticle suspension was adjusted to a concentration of 0.01 wt % in deionized water or in 0.01 mol/L sodium chloride solution for ζ potential examination. All analyses were done three times, and the results are the average of three runs.

Scanning electron microscopy (SEM) observation

The surface morphology of the CS–PAA nanoparticles was observed with a Jeol 3100 scanning electron microscope (Tokyo, Japan) at 25 kV. The platinum-coated particle surface was prepared under an argon atmosphere.

X-ray diffraction (XRD) analysis

The crystal structure of CS–PAA nanoparticle was determined with a Rigaku D/max3 Vx X-ray diffractometer (Tokyo, Japan) at a scanning rate of 4°/min for 2θ values from 10 to 50°.

Adsorption experiments

A stock solution (1000 ppm) of nickel ion was prepared with nickel nitrate (Riedel-de Haën). The stock solution was then diluted to give a standard solution of appropriate concentration. Batch experiments were conducted in 250-mL beakers and equilibrated with a magnetic stirrer. Then, 100-mL aliquots of these standard solutions were placed in 250-mL beakers, and CS–PAA nanoparticles were added.

In the adsorption equilibrium experiments, 0.10 g of CS–PAA nanoparticles and 100 mL of nickel solution buffered at pH 5 containing several concentrations of Ni(II) ions were used. The system was maintained under shaking at 25°C until the adsorption equilibrium was reached. Nickel ion uptake experiments were conducted in the range pH = 3–7 by the addition of 1M hydrochloride or 1M sodium hydroxide as required. After equilibration, the nickel nitrate solutions were filtered through papers and quantified by a GBC Scientific Equipment SensAA Flame atomic absorption spectrophotometer (Melbourne, Australia). The adsorption capacities of the nickel ions taken up by the sorbent in each flask were determined by the following mass balance equation:

$$Q = \frac{(C_0 - C_e)V}{W} \quad (1)$$

where Q is the sorption capacity (mg/g); C_0 and C_e are the initial and solution-phase nickel ion concentrations at equilibrium (ppm), respectively; V is the solution volume (L); and W is the mass of sorbent (g)

For batch kinetic studies, the CS–PAA nanoparticle and 100 mL of nickel ion solutions with different initial concentrations were placed in 250-mL beakers and stirred by a magnetic stirrer. Different amounts of CS–PAA nanoparticles with different mean particle sizes were placed in 250 mL of the nickel solution with shaking for 24 h at 260 rpm; this was expected to provide information about the optimum conditions for adsorption of Ni ions. The sorption time was varied between 10 and 100 min. During the kinetic experiments, samples were withdrawn at fixed time intervals, filtered, and quantified by the Flame atomic absorption spectrophotometer.

Isotherm studies were conducted with a constant CS–PAA nanoparticle weight (0.10 g) and various initial concentrations of nickel ions in the range 40–100 ppm.

RESULTS AND DISCUSSION

Particle size and structure of the CS–PAA nanoparticles

The preparation of the CS–PAA nanoparticles was based on an electrostatic-induced interaction between

TABLE I
Mean Particle Size and ζ Potential of CS–PAA Complex Nanoparticles at Different
CS : PAA Volume Ratios and pH Values

Sample	pH	CS : PAA (w/w)	Mean diameter (nm)	Polydispersity	ζ potential (mV)
I	3	1 : 1	35 ± 8	0.0522	33.5 ± 0.4
II	5	1 : 2	194 ± 8	0.0717	18.6 ± 0.6
III	5	1 : 1	175 ± 14	0.0491	20.1 ± 0.7
IV	5	2 : 1	100 ± 11	0.0801	20.6 ± 0.8
V	7	1 : 1	638 ± 112	0.1752	10.8 ± 0.5

positively charged CS and negatively charged PAA at room temperature.[18] Adjusting the final solution pH value directly instead of during the incubation process changed the incubation process for the modified CS–PAA nanostructure. The CS–PAA nanoparticles prepared in the experiment had a white powder shape and were insoluble in water and dilute acid.

CS–PAA nanoparticles produced at a solution pH of 4.5 were tested for their size and ζ potential response to changing pH values of the residing solution medium by simple adjustment of the solution pH from 3 to 7. Table I shows the results of the mean diameter and surface charge of the CS–PAA nanoparticles with the CS:PAA volume ratio fixed at 1 under different pH values. Both measured particle size and ζ potential were very sensitive to the change in pH values of the residing aqueous environment, which indicated that the surface density of the protonized amino groups and the degree of protonation were reversibly responsive to changing solution pH values. The increase in measured average particle size could have been caused mainly by particle aggregation when the solution pH value increased. Apparently, the diameter of the nanoparticles increased with increasing pH from 3 to 7. The increase in size at pH 7 suggested that the degree of protonation at the surfaces of the particles was reduced, which decreased the electrostatic repulsion between the particles and, thereby, increased the probability of particle aggregation. An extremely small size of the CS–PAA nanoparticles (about 35 nm) could be obtained at pH 3. However, the high positive charge of these nanoparticles did not favor metal chelating. Thus, the final pH value of the CS–PAA nanoparticle solution was changed to 5 for further adsorption experiments.

The particle size distributions and surface charges of the CS–PAA nanoparticles with various CS : PAA volume ratios was also characterized by the Zetasizer at pH 5. The results are also shown in Table I. The mean diameter of the nanoparticles ranged from 100 to 194 nm with a narrow size distribution. With increasing CS:PAA volume ratio, the mean size of the nanoparticles decreased. The surfaces of the CS–PAA nanoparticles had positive charges of about 20–30 mV. Table I also shows that as the ratio of

CS : PAA increased, the ζ potential also increased. As the content of CS exceeded that of PAA, some of the excessive CS was absorbed onto the surface of the CS–PAA nanoparticles. The excess CS increased the surface charges of the CS–PAA nanoparticles and resulted in an increase in the ζ potential.

Morphology of the CS–PAA nanoparticles

Figure 1 shows the SEM image of pH 5 modified CS–PAA nanoparticles obtained at a CS:PAA volume ratio of 2 : 1. It exhibits aggregates composed of adjacent nanoparticles with a microporous structure. According to our previous study, when the pH values are between 4.5 and 5.8, CS and PAA are partly ionized and form a polyelectrolyte complex by ionic interaction, which leads to a microporous structure with solid in consistent spherical shapes. The microporous structure of CS–PAA favors the sorption of nickel ions.[6]

Figure 2 illustrates TEM images of pH 5 modified CS–PAA nanoparticles obtained at a CS:PAA volume ratio of 2 : 1. It was clear that CS–PAA particles were essentially monodisperse and had a similar mean diameter of 100 nm. The TEM photographs demonstrated that most of the nanoparticles were solid in consistent spherical shapes.
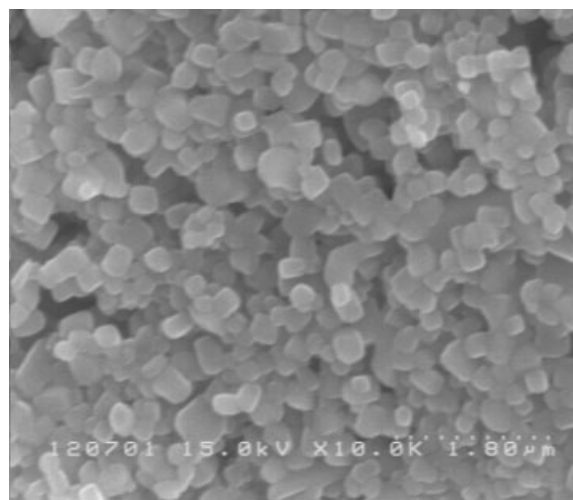

Figure 1 SEM image of pH 5 modified CS–PAA nanoparticles obtained at a CS : PAA volume ratio of 2 : 1.
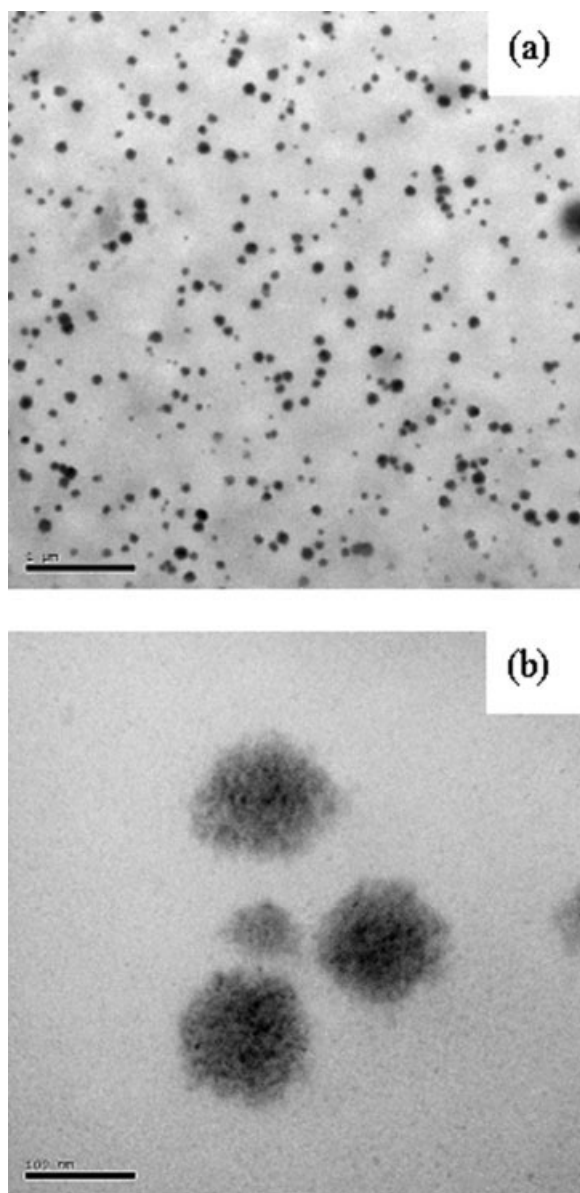
Figure 2 TEM images of pH 5 modified CS–PAA nanoparticles obtained at a CS : PAA volume ratio of 2 : 1: (a) 20,000× and (b) 200,000×.

Intermolecular interaction between the components

The FTIR–ATR spectra of PAA, CS, and the CS–PAA nanoparticles with different pH values are shown in Figure 3. For CS, the intensities of the amide I band at 1665 cm^{-1} and amide II band at 1580 cm^{-1} were observed clearly. The basic characteristics of CS at 3450 cm^{-1} (OH stretching and N—H stretching) and 2920 cm^{-1} (C—H stretching on methyl) were also observed. However, in the CS–PAA nanoparticles, the two characteristic peaks of CS decreased dramatically, and a new absorption band at 1705 cm^{-1}, which could be assigned to the absorption peaks of the carboxyl groups of PAA (the absorption peak of

carboxyl groups in pure PAA appeared at 1750 cm^{-1}) was observed. The broad peak appeared at 2500 cm^{-1}, which confirmed the presence of NH$_3^+$ in the CS–PAA nanoparticles. In addition, the absorption peaks at 1450 and 1408 cm^{-1} were assigned to asymmetric and symmetric stretching vibrations of COO$^-$ anion groups. These results indicate that the carboxylic groups of PAA were dissociated into COO$^-$ groups, which complexed with protonated amino groups of CS through electrostatic interactions to form the polyelectrolyte complex during the mixing procedure.

The FTIR–ATR spectra of the pH modified CS–PAA nanoparticles are also shown in Figure 3. The intensity of a new adsorption band at 1705 cm^{-1}, which was assigned to the absorption peaks of the carboxyl groups of PAA, decreased dramatically with increasing
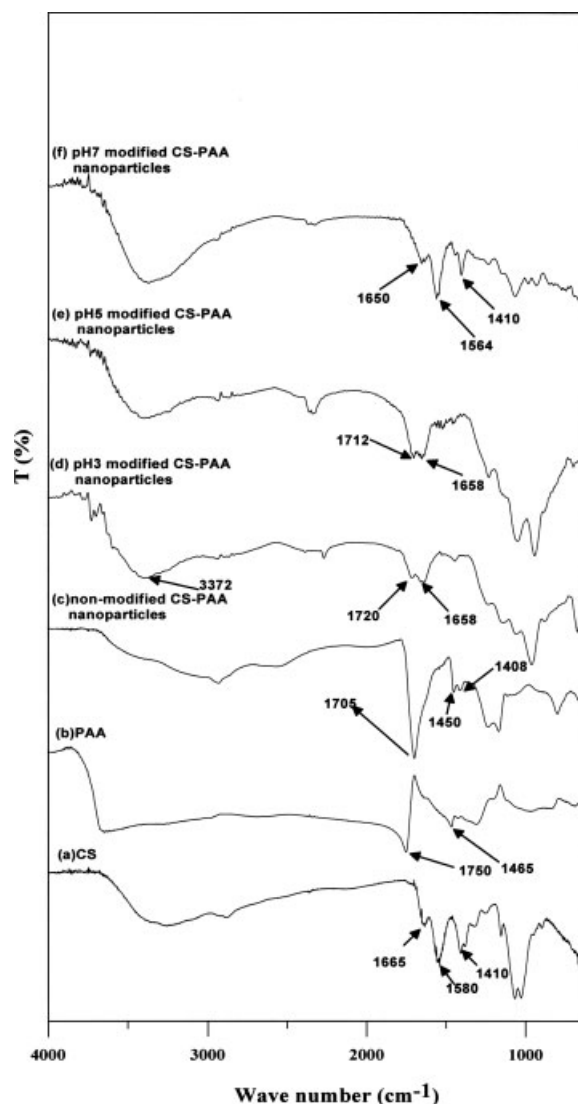

Figure 3 FTIR–ATR spectra of (a) CS, (b) PAA, and (c) nonmodified, (d) pH 3 modified, (e) pH 5 modified, and (f) pH 7 modified CS–PAA nanoparticles. T, transmittance.
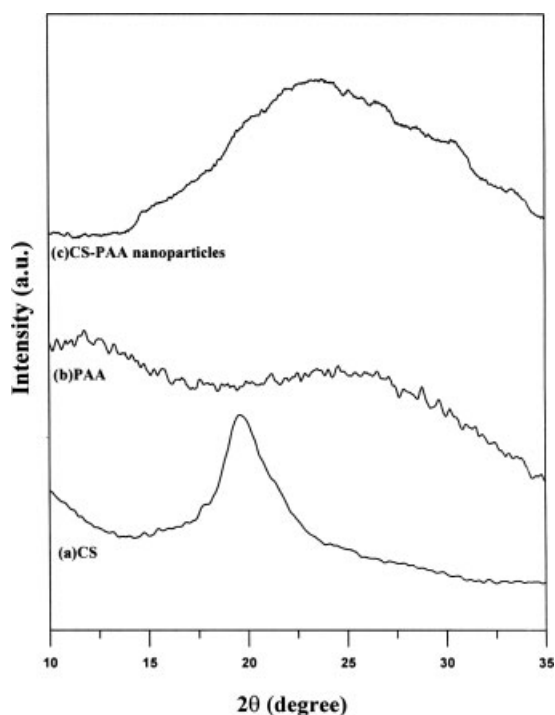
Figure 4 XRD patterns of (a) CS, (b) PAA, and (c) pH 5 modified CS–PAA nanoparticles.

pH value of the CS–PAA solution. The presence of the amide II band increased as the pH value was increased to 7, which indicated that some amine groups from CS were in the NH_2 form. At this pH, PAA was highly swollen, whereas CS was insoluble. (The pK_a values of PAA and CS were 4.75 and 6.50, respectively),[19] which resulted in the phase separation of nanoparticles; that is, the CS was just physically coated on the CS–PAA nanoparticles. Thus, under neutral conditions, the CS–PAA nanoparticles would be destroyed, which would result in an aggregation of CS due to its insolubility in neutral solution.

Crystallinity of the CS–PAA nanoparticles

Figure 4 shows the XRD patterns of the CS, PAA, and the CS–PAA nanoparticles, in which a broad reflection peak was obtained for CS and PAA, which indicated that both CS and PAA had an inferior crystallinity. The XRD pattern of CS showed the characteristic peak at 2 θ = 20°, which indicated the presence of (101) and (002). The peak at 20° was the allomorphic tendon form of CS, which resulted in a strong decrease in the sorption capacities.[20] However, in the XRD pattern of the CS–PAA nanoparticles, we found that the reflection peak of the CS disappeared, but another broad reflection peak was found at 2 θ = 23.82°, which showed that a cross-linked reaction occurred. The new polymer complex had an inferior crystallinity, which means that it was

amorphous, not crystalline. When a polymer complex between CS and PAA is formed, the amino and hydroxyl groups in the CS react with the carboxylic groups of PAA. This reaction breaks the hydrogen bonding between the amino groups and hydroxyl groups in the CS and then leads to an amorphous structure in the CS–PAA polymer complex.[21] Many studies have shown that the sorption may be restricted to external layers. This may be explained by diffusion limitations and, more specifically, by resistance to intraparticle diffusion. However, it is not the only cause. Piron et al.[22] showed that decreasing the crystallinity of CS results in an improvement in the metal ion sorption properties. They prepared different forms of the polymer by dissolving CS followed by freeze drying to break the crystallinity of the raw material without recrystallization and confirmed that the low crystallinity of CS allowed rapid sorption rates and high sorption capacities. The CS–PAA nanoparticle also exhibited lower crystallinity due to the freeze-drying procedure. As a result, the nickel sorption rate improved significantly.

Adsorption of CS–PAA nanoparticles for Ni ions

Adsorption isotherms

To examine the relationship between sorbed (Q) and aqueous concentrations (C_e) at equilibrium, sorption isotherm models are widely employed to fit the data, of which the Langmuir and Freundlich equations are the most widely used. To get the equilibrium data at pH 5 and room temperature, initial metal concentrations were varied, whereas the biomass weight in each sample was kept constant. Figure 5 shows the experimental equilibrium isotherms for the sorption of nickel ions by the CS–PAA nano-
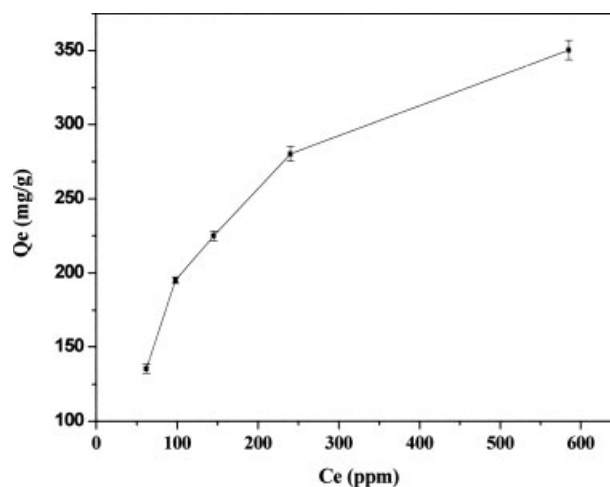

Figure 5 Ni^{2+} sorption isotherm by the CS–PAA nanoparticles (sorbent dosage = 100 mg, particle mean size = 100 nm, pH 5).
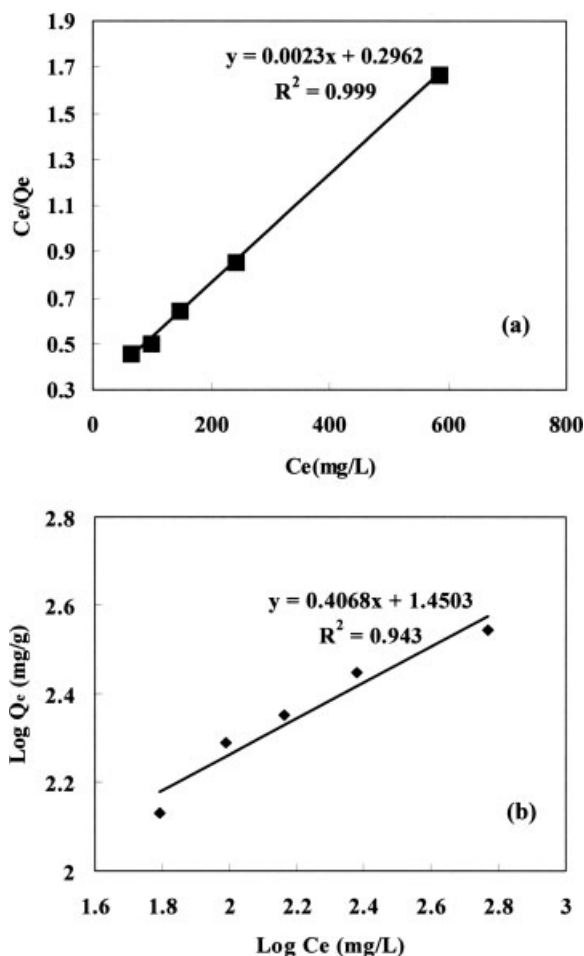
Figure 6 (a) Langmuir and (b) Freundlich plots for Ni^{2+} uptake by the CS–PAA nanoparticles (sorbent dosage = 100 mg, particle mean size = 100 nm, pH 5).

particles. The experiment showed that the sorption capacity increased with increasing initial concentration of nickel ions. When the concentration of nickel ions at equilibrium was 585 ppm, the sorption capacity reached 350 mg/g, which was a considerable improvement over that of CS.[23]

The Langmuir isotherm is based on the assumption of monolayer adsorption onto a surface containing a finite number of adsorption sites of uniform energies of adsorption with no transmigrates of adsorbate in the plane of the surface. The experimental data were fitted to the Langmuir isotherm:

$$\frac{C_e}{Q_e} = \frac{C_e}{Q_{max}} + \frac{1}{Q_{max}b} \tag{2}$$

where C_e is the equilibrium concentration of nickel ions (ppm), Q_e is the amount of nickel ions sorbed per unit weight of CS–PAA nanoparticles at equilibrium (mg/g), Q_{max} is the maximum amount adsorbed on a monolayer (mg/g), and b is the Langmuir sorption equilibrium constant (mL/mg), which is a measure of the energy of sorption. A linearized plot of C_e/Q_e against C_e gave Q_{max} and b [Fig. 6(a)]. The results obtained were Q_{max} = 435 mg/g and b = 0.0078 ppm. The equation was $C_e/Q_e = C_e \times 0.0054 + 0.7186$. The plots demonstrated that the Langmuir equation provided a reasonable description of the experimental data.

To a lesser extent, the equilibrium data were also well described with the Freundlich equation, probably due to the real heterogeneous nature of the surface sites involved in the metal uptake.[24] The widely used empirical Freundlich equation, based on sorption by a heterogeneous surface is

$$\log Q_e = \left(\frac{1}{n}\right) \log C_e + \log k \tag{3}$$

where k and n are Freundlich constants indicating sorption capacity and intensity, respectively. k and n can be determined from a linear plot of $\log Q_e$ against $\log C_e$ [Fig. 6(b)]. The calculated results of the Langmuir and Freundlich isotherm constants are given in Table II. The adsorption of nickel ions by the CS–PAA nanoparticle correlated well (correlation coefficient (R^2) = 0.999) with the Langmuir equation as compared to the Freundlich equation (R^2 = 0.9432) under the concentration range. The magnitudes of k and n showed easy separation of Ni(II) ions from the aqueous medium and indicated favorable adsorption. As shown in Table II, n values were high enough for the separation of heavy-metal ions from the aqueous medium. The conformity of the adsorption data to the Langmuir isotherm (correlation coefficient > 0.95) could be interpreted as indicating a homogeny adsorption process, leading to monolayer binding. The essential features of a Langmuir isotherm can be expressed in terms of a dimensionless constant separation factor or equilibrium parameter (R_L), which is used to predict whether an adsorption system is favorable or unfavorable. R_L is defined as follows:[25]

$$R_L = \frac{1}{1 + bC_0} \tag{4}$$

TABLE II
Parameters of the Langmuir and Freundlich Isotherms for the Adsorption of Ni(II) on the CS–PAA Nanoparticles

Metal	Langmuir			Freundlich		
	Q_{max} (mg/g)	b (mL/mg)	Correlation coefficient	k	n	Correlation coefficient
Ni(II)	435	0.0078	0.9990	28.2033	2.1701	0.9430

R_L Values Based on the Langmuir Equation

C_0 (mg/L)	R_L
70	0.646831
100	0.561798
150	0.460829
250	0.338983
600	0.176056

where C_0 is the initial Ni^{2+} concentration (ppm) and b is the Langmuir adsorption equilibrium constant (mL/mg). Table III lists the calculated results. R_L values in the range $0 < R_L < 1$ indicated that the CS–PAA nanoparticles were favorable adsorbents for Ni(II) removal from the aqueous solution.

Adsorption kinetics

Effect of initial nickel concentration. Sorption kinetics are important physicochemical parameters for the evaluation of the basic qualities of a good sorbent. The removal of nickel ions by the CS–PAA nanoparticles as a function of time at pH 5 at various initial concentrations (40–100 ppm) is shown in Figure 7. The results indicate that at higher initial concentrations of nickel ions, it took more time to reach equilibrium, and there was a lower sorption percentage. When the initial concentration of nickel ions was 40 ppm, the sorption percentage reached 88% at 10 min, the sorption amount was 70 mg/g, and the equilibrium time was just 30 min. When the initial concentration of nickel ions increased to 100 ppm, the sorption percentage was 75% at 10 min, and the sorption amount was 150 mg/g. The sorption reached equilibrium after 90 min, the sorption
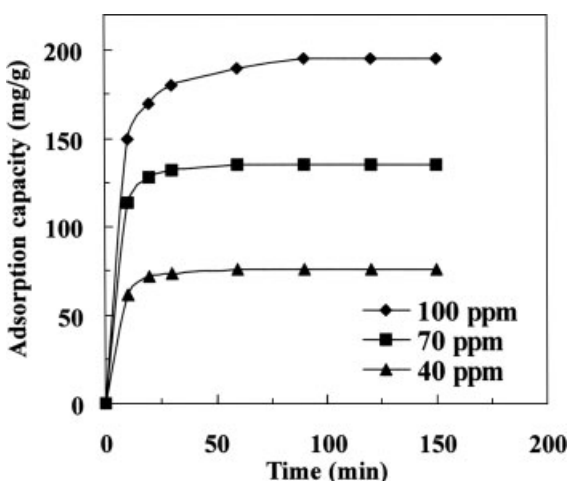
amount reached 195 mg/g, and the sorption percentage increased to 98%. To evaluate the mechanism of adsorption kinetics, the pseudo-first-order and pseudo-second-order were tested to interpret the experimental data. The pseudo-first-order kinetic model[26] is given as follows:

$$\log(Q_e - Q_t) = \log Q_e - \frac{k_1}{2.303}t \tag{5}$$

where Q_e is the amount of sorbate adsorbed per unit weight of sorbent at equilibrium (mg/g), Q_t is the amount of sorbate uptake per unit weight of sorbent at any time t (mg/g), t is the time (min), and k_1 is the adsorption rate constant of pseudo-first-order (min^{-1}). The values of k_1 were calculated from the slopes of the plot of log ($Q_e - Q_t$) versus t. The pseudo-second-order equation[27] may be expressed as follows:

Figure 7 Effect of the initial concentration of nickel ions on the sorption kinetics of the CS–PAA nanoparticles (sorbent dosage = 50 mg, particle mean size = 100 nm, pH 5).
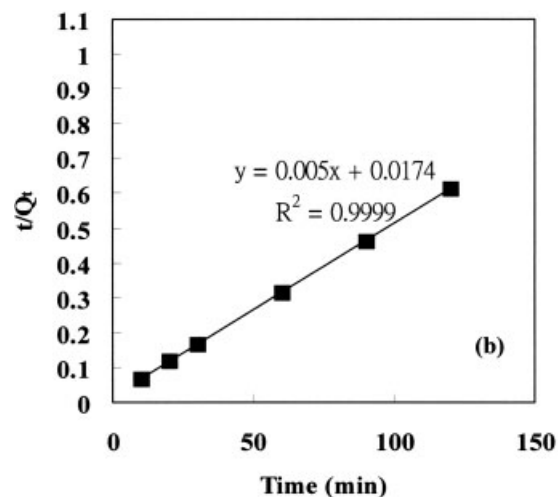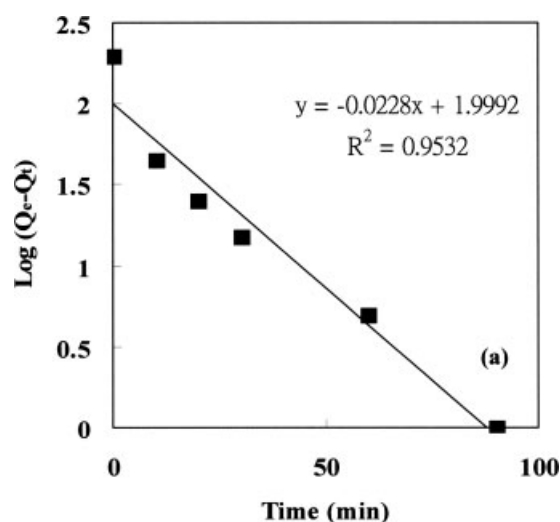

Figure 8 Linearization of adsorption kinetics: (a) pseudo-first-order and (b) pseudo-second-order model (sorbent dosage = 50 mg, particle mean size = 100 nm, initial concentration of nickel ions = 100 ppm, pH 5).
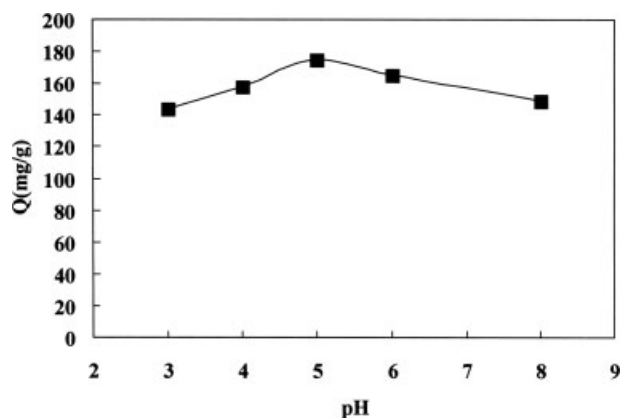
Figure 9 Effect of pH on the adsorption of nickel ions by the CS–PAA nanoparticles (sorbent dosage = 50 mg, particle mean size = 100 nm, initial concentration of nickel ions =100 ppm).

$$\frac{t}{Q_t} = \frac{1}{k_2 Q_e{}^2} + \frac{t}{Q_e} \quad (6)$$

where k_2 is the pseudo-second-order adsorption rate constant (g/mg min). The validity of this model could be interpreted by linear plots of t/Q_t versus t. As shown in Figure 8(a,b), the correlation coefficients (R) given by these two kinetic models between the predicted and the experimental values were 0.9532 and 0.9999, respectively. Obviously, the pseudo-second-order kinetic model, in contrast to the pseudo-first-order, gave a good correlation for the adsorption of nickel ions by the CS–PAA nanoparticles. This suggests that the rate-limiting step may be the chemical adsorption, not the mass transport limitation. Increasing metal ion concentration in the aqueous solution seemed to reduce the external diffusion of the adsorbent and enhanced intraparticular diffusion.[28]

Effect of pH value. Figure 9 shows the relationship between the pH value in the original solution and the adsorption capacity for nickel ions. The adsorption of nickel reached a maximum at pH 5 and decreased at lower and higher pH values. Low pH favored the protonation of the amino sites, which resulted in a reversal of charge and greatly diminished the metal chelating ability of CS. In acidic solutions, more protons were available to protonate amine groups to form —$NH_3{}^+$ groups, which reduced the number of binding sites for the adsorption of nickel. Heavy-metal cations are completely released under extremely acidic conditions Although, at higher pH values beyond 6.5, the precipitation of nickel hydroxide occurred simultaneously with the sorption of nickel ions, which affected the sorption by the CS nanoparticles. The other reasons for the decrease of nickel adsorption with increased pH were the aggregation of nanoparticles and, related to this, a decrease in surface area.

Effect of the amount of nanoparticles. We studied the dependence of the adsorption of Ni(II) on the amount of CS–PAA nanoparticles at room temperature and at pH 5 by varying the nanoparticle amount from 0.02 to 0.05 g (mean size = 100 nm) in contact with 50 mL of nickel ion solution. The results are shown in Figure 10. Apparently, the percentage removal of nickel ions increased with increasing nanoparticles due to the greater availability of the adsorbent. The adsorption reached a maximum with 0.05 g of CS–PAA nanoparticles, and the maximum percentage removal was about 98% for nickel ions.

Effect of the mean size of the nanoparticles. Figure 11 shows the sorption kinetics obtained at differing sizes of CS–PAA nanoparticles. This indicates that the higher sorption capacity was achieved as the mean size of the CS–PAA nanoparticles decreased. CS–PAA nanoparticles with a mean size of 100 nm had a high sorption capacity of 195 mg/g when in contact with a 100 ppm nickel ion solution. Increasing the size of the nanoparticles also increased the
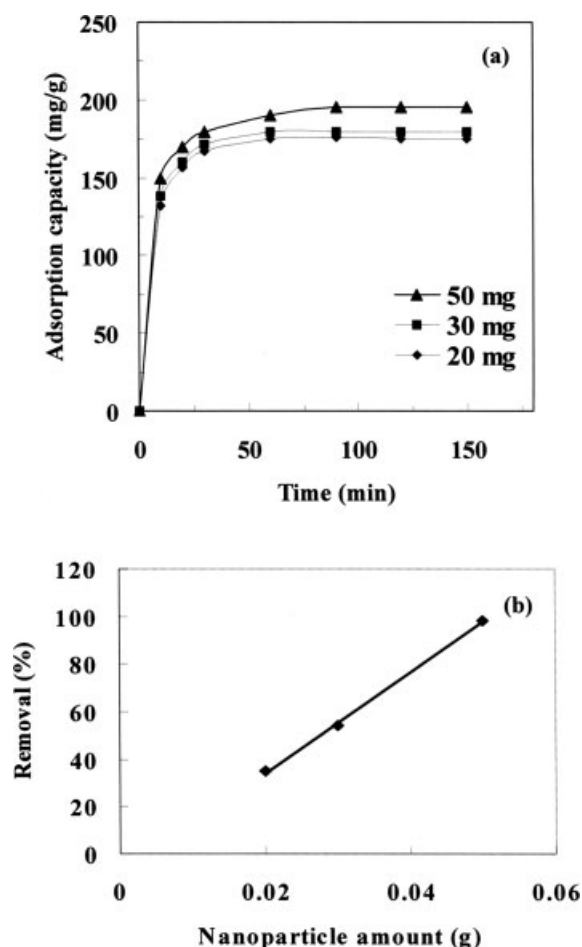

Figure 10 Effect of the amount of nanoparticles on (a) the nickel sorption capacity and (b) the nickel removal percentage (particle mean size = 100 nm, initial concentration of nickel ions = 100 ppm, pH 5).
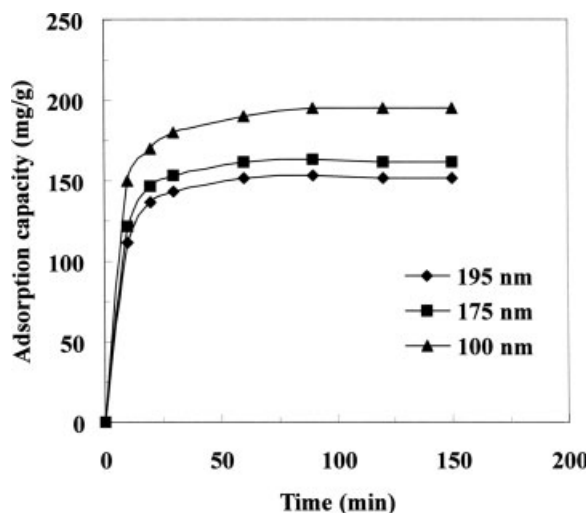
Figure 11 Effect of the mean size of the CS–PAA nano-particles on nickel sorption (sorbent dosage = 50 mg, initial concentration of nickel ions = 100 ppm, pH 5).

time required to reach equilibrium. This result was similar to Qi and Xu,[6] who studied the sorption behavior of CS–tripolyphosphate nanoparticles for lead ions. The contact surfaces of small-size nanoparticles could explain the differences among various mean sizes of nanoparticles for nickel sorption. The sorption performance of the CS–PAA nanoparticles could have been affected significantly by the particle size and conditioning of the adsorbent due to the diffusion restrictions caused by the low porosity and crystallinity of the raw CS.[29] CS–PAA nanoparticles reduced the crystallinity of the biopolymer and led to the expansion of the polymer network to increase the accessibility to internal sites and sorption rates.

CONCLUSIONS

A self-assembling process synthesizing large quantities of uniform CS–PAA nanoparticles by a pH-modified dropping method was successfully developed in this study. The diameter of the CS–PAA nanoparticles could be easily controlled by the pH value of the solution and the CS : PAA volume ratio. By adjusting the final pH value of the CS solution to 5 and then dropping CS into the PAA solution at a volume ratio of 2 : 1, we obtained yields of nanoparticles of 100 nm in the suspension solution.

The CS–PAA nanoparticles had a weak and broad peak at $2\theta = 23.82°$, which showed the amorphous characteristics of the nanoparticles. The low crystallinity of the CS–PAA nanoparticles was responsible for their sorption efficiency. The sorption rate was affected significantly by the initial concentration of the solution, sorbent amount, size, and pH value of the solution. The CS–PAA nanoparticles 100 nm in diameter were efficient as nanoadsorbents for the

fast and maximum adsorption of nickel ions from aqueous solutions at pH 5 due to high specific surface area and the absence of internal diffusion resistance. The equilibrium adsorption data were correlated by the Langmuir and Freundlich isotherm equations. The maximum monolayer adsorption capacity of the CS–PAA nanoparticle was 435 mg/g for nickel ions. The kinetic experimental data correlated well with the pseudo-second-order kinetic model. Nickel (CS–PAA nanoparticle) sorption would be worthy of further investigation to explore its high-capacity advantage.

References

1. Vieira, R. S.; Beppu, M. M. Water Res 2006, 40, 1726.
2. El-Shafey, E.; Cox, M.; Pichugin, A. A.; Appleton, Q. J Chem Technol Biotechnol 2002, 77, 429.
3. Babel, S.; Kurniawan, T. A. J Hazard Mater 2003, 97, 219.
4. Krajewska, B. Sep Purif Technol 2005, 41, 305.
5. Hu, J.; Chen, G. H.; Lo, I. M. C. Water Res 2005, 39, 4528.
6. Qi, L.; Xu, Z. Colloids Surf A 2004, 251, 183.
7. Chang, Y. C.; Chen, G. D. H. Macromol Biosci 2005, 5, 254.
8. Chang, Y. C.; Chen, D. H. J Colloid Interface Sci 2005, 283, 446.
9. Mao, H. Q.; Roy, K.; Troung-Le, V. L.; Janes, K. A.; Lin, K. Y.; Wang, Y. J.; August, T. K.; Leong, W. J Controlled Release 2001, 70, 399.
10. Tiyaboonchai, W.; Woiszwillo, J. C.; Middaugh, R. Eur J Pharm Sci 2003, 19, 191.
11. Bodmeier, R.; Chen, H.; Paeratakul, O. Pharm Res 1989, 6, 413.
12. Lin, Y. H.; Chung, C. K.; Chen, C. T.; Liang, H. F.; Chen, S. C.; Sung, H. W. Biomacromolecules 2005, 6, 1104.
13. Douglas, K. L.; Tabrizian, M. J Biomater Sci Polym Ed 2005, 16, 43.
14. Alonso-Sande, M.; Cuna, M.; Remunan-Lopez, C. Macromolecules 2006, 39, 4152.
15. Kabanov, V. A.; Yaroslavov, A. A.; Sukhishvili, S. A. J Controlled Release 1996, 39, 173.
16. Schatz, C.; Lucas, J. M.; Viton, C.; Domard, A.; Pichot, C.; Delair, T. Langmuir 2004, 20, 7766.
17. Chang, T. C.; Wang, J. W.; Hon, M. H. Macromol Biosci 2004, 4, 416.
18. Hu, Y.; Jiang, X.; Ding, Y.; Ge, H.; Yuan, Y.; Yang, C. Biomaterials 2002, 3, 3193.
19. Lee, J. W.; Kim, S. Y.; Kim, S. S.; Lee, Y. M.; Lee, K. H.; Kim, S. J. J Appl Polym Sci 1999, 73, 113.
20. Chassary, P.; Vincent, T.; Guibal, E. React Funct Polym 2004, 60, 137.
21. Ann, J. S.; Choi, H. K.; Cho, C. S. Biomaterials 2001, 22, 923.
22. Piron, E.; Accominotti, M.; Domard, A. Langmuir 1997, 13, 1653.
23. Kalyani, S.; Priya, J. A.; Rao, P. S.; Krishnaiah, A. Sep Sci Technol 2005, 40, 1483.
24. Reddad, Z.; Gerete, C.; Andres, Y.; Ralet, M. C.; Thibault, J. F.; Le Cloirec, P. Carbohydr Polym 2002, 49, 23.
25. Wan Ngah, W. S.; Endud, C. S.; Mayanar, R. React Funct Polym 2002, 50, 181.
26. Chiou, M. S.; Li, H. Y. Chemosphere 2003, 50, 1095.
27. Wan Ngah, W. S.; Ab Ghani, S.; Kamari, A. Bioresour Technol 2005, 96, 443.
28. Vilar, V. J. P.; Botelho, C. M. S.; Boaventura, R. A. R. Process Biochem 2005, 40, 3267.
29. Guibal, E.; Jansson-Charrier, M.; Saucedo, I.; Le Cloirec, P. Langmuir 1995, 11, 591.